Scanning Electron Microscopy

Volume 3
Number 1 *3rd Pfefferkorn Conference*

Article 14

1984

Field Emission Source Optics

L. W. Swanson
Oregon Graduate Center

Electron Optical Systems (pp. 137-147)
SEM Inc., AMF O'Hare (Chicago), IL 60666-0507, U.S.A.

0-931288-34-7/84$1.00+.05

FIELD EMISSION SOURCE OPTICS

L. W. Swanson

Department of Applied Physics and
Electrical Engineering
Oregon Graduate Center
19600 N.W. Walker Road
Beaverton, Oregon 97006

Phone no.: (503) 645-1121

Abstract

The use of field emission processes as a means of generating high brightness sources of both electrons and ions is becoming of increasing practical use in electron/ion optical systems. A review is given of the source optics and emission characteristics of a zirconium oxide coated, <100> oriented, tungsten (ZrO/W(100)), thermal field emitter electron (TFE) source and a liquid metal ion source (LMIS). The primary interest at present is the use of these high field sources in microprobe focusing columns where beam sizes of < 0.5 μm and target current densities of ~ 1 to 10 A/cm^2 (in the case of a LMIS) and 10^2 to 10^4 A/cm^2 (in the case of a ZrO/W(100) TFE) are required. For predicting the performance of field emission sources in microprobe columns source properties such as beam energy spread (ΔE), angular intensity (I') and virtual source size (d_v) are of interest. For the LMIS experimental values of ΔE, I' and d_v are found to depend on particle charge to mass ratio and total source current. Similarly for the ZrO/W(100) TFE experimental values of ΔE increase with I'. A computer program, known as SCWIM, has been designed to model point-to-plane source geometries and is used to model such emitter parameters as d_v and I'.

Key words: Field Emission, Liquid Metal Ion Source, Field Ionization, High Brightness.

Introduction

High field sources for the formation of both electrons and ions are becoming of increasing importance in optical systems used to form high current density, focused beams of size < 0.5 μm. A field emission mechanism is common to both ion (e.g., gas phase field ionization and solid or liquid phase field evaporation) and electron formation where a conically shaped emitter of radius r < 1 μm is typically employed to achieve the high field strengths. Since field emission involves a quantum mechanical tunnelling process it can theoretically occur at T = 0 K. Nevertheless for various reasons the emitters usually operate at elevated temperature thereby resulting in a thermal-field (TF) operating mode.

For field electron emission analytical expressions governing the relationships among cathode electron energy distribution, current density, work function ϕ, surface electric field F and temperature T have been developed [13]. In contrast, for ion formation via field evaporation or field ionization the theoretical model is less well developed in terms of the current density $J_c(F,\phi,T)$ and full width at half maximum (FWHM) of the total energy distribution $\Delta E(F,\phi,T)$ relationships. Nevertheless important source optic characteristics such as $\Delta E(F,T)$, the angular intensity $I' = dI/d\Omega$ (where Ω is the solid angle of emission) and the virtual source size d_v can be either measured experimentally [1,8,9] or obtained from computer analysis of emitter/extractor electrode geometry [5]. In this study we shall examine these source optical parameters for two promising, high brightness emitters: the zirconium oxide/W(100) TF electron (TFE) source for electrons and the liquid metal ion source (LMIS). The results of a computer program SCWIM [3,4] especially designed to compute trajectories and d_v values for point-to-plane electrode geometries will be discussed.

Source Optics

The source optical characteristics of primary importance for the formation of high current density focused beams using high field sources are summarized in Table 1. Figure 1 depicts the typical geometry and trajectory relationships for the hemisphere on cone type high field source. The angular magnification m is given by

List of Symbols

B_A - apparent axial brightness
C_c - chromatic aberration coefficient
D_s - spherical aberration coefficient
d - focused beam size
d_v - virtual source diameter
D(w) - transmission coefficient
E_F - Fermi level
ΔE - full width at half maximum of energy distribution
F - electric field
f - facet radius
h_θ - angular mesh size
I' - angular intensity
J_A - apparent current density
J_c - cathode current density
J(E) - current density per unit energy
m - angular magnification
m' - linear magnification
N - no. radial mesh points
r - emitter radius or radial distance
r_g - radius of Gaussian image disk
r_s - radius of emission disk on cathode
R_m - maximum mesh radius
R_o - minimum mesh radius
T - temperature
V - beam voltage
W - normal energy

α - beam angle
ε - energy relative to Fermi level
ε_o - permittivity of free space
λ - deBroglie wavelength
ϕ - work function
ρ - charge density
θ - emission angle

$$m = \frac{d\alpha}{d\theta} \tag{1}$$

and d_v can be determined from knowledge of the trajectories. In addition d_v can be determined experimentally, although such experiments are difficult to carry out. If m is known then the following relationship between I' and the cathode current density J_c

$$I' \tilde{=} \frac{J_c r^2}{m^2}, \tag{2}$$

can be derived for small values of α where r is the emitter radius. Usually I' is easily obtained experimentally whereas the predicted value of J_c requires knowledge of the surface electric field and the theoretical emission relationship $J_c(F,\phi,T)$.

The radius of a disk on the cathode r_s is related to a corresponding Gaussian image disk r_g by

$$r_g = M' r_s \tag{3}$$

where M' is the linear magnification. From these fundamental parameters other source characteristics such as apparent current density

$$J_A = 4I'\alpha^2/d_v^2$$

and apparent axial brightness

$$B_A = J_A/\pi\alpha^2 \tag{4}$$

can be derived.

For a single lens system the focused beam size d is given by

$$d = M\left[d_v^2 + \left(\frac{1}{2} C_s \alpha^3\right)^2 + \left(C_c \alpha \frac{\Delta E}{eV}\right)^2 + \left(0.6 \frac{\lambda}{\alpha}\right)^2\right]^{1/2} \tag{5}$$

where the spherical and chromatic aberration coefficients C_s and C_c are referred to the object side, M is the column magnification and λ is the particle wave length. The importance of ΔE and I' can be illustrated for the focused beam case when d_v and chromatic aberration disks dominate the aberration terms. In this case it can be shown that the beam current I_b is given by:

$$I_b = \left(\frac{d^2}{M^2} - d_v^2\right)\left(\frac{eV}{\Delta E C_c}\right)^2 I'\pi \tag{6}$$

Thus for a specified value of d the beam current is proportional to the source parameter $I'/\Delta E^2$. In addition, I_b is proportional to $d^2/M^2 - d_v^2$. This simple example illustrates the importance of the source parameters I', ΔE and d_v.

Computation of Electric Potential and Trajectories

In order to obtain the field required for high current density at convenient voltages, the emitter is usually much smaller in comparison to the size of other electrodes. This difference can be as large as 10^7, as in the case of a field ion emitter, and is normally in excess of 10^3. To complicate matters the emitter shape may be non-hemispherical depending on the operating condition. For example a faceted shape frequently occurs in the case of TF emission due to field build up [4]. To deal with this problem a special coordinate system was employed known as SCWIM (spherical coordinate with increasing mesh size) [3,4].

Figure 2 is a schematic representation of the SCWIM model. The radial mesh size increases from the emitter outward according to a geometrical series with a term ratio $(1 - h_\theta)^{-1}$, where h_θ is the angular mesh size, in radians. If one

TABLE 1

Summary of source characteristics and their effect on focused beam optics. Optics column magnification, chromatic aberration, source angular magnification, emitter apex radius and aperture half angle are M, C_c, m, r and α, respectively.

Source Characteristics	Optics Function	Quantitative Effect
Angular Intensity $I'(F,\phi,T)$	Determines Beam Current	$I'\pi\alpha^2$
Virtual Source Size $d_v(\alpha,r,F)$	Determines Minimum Beam Size	Md_v
Beam Energy Spread $\Delta E(F,\phi,T)$	Determines Minimum Chromatic Aberration Disk	$MC_c\alpha\frac{\Delta E}{eV}$
Emitter Current Density J	Determines I'	Jr^2/m^2

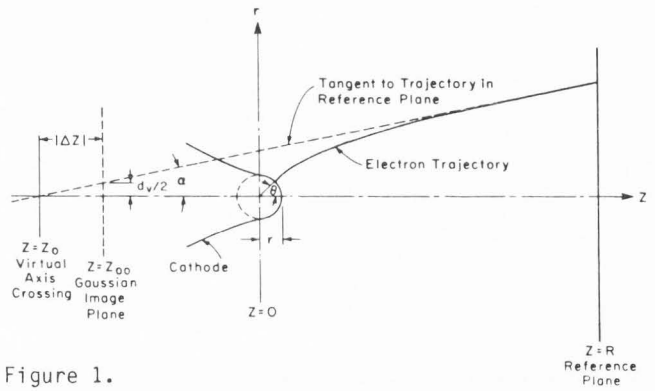

Figure 1.

Illustration of a typical trajectory and position of virtual axis crossing relative to Gaussian image plane.

takes h_θ on both sides to be the same, then a quasi-equidistant central difference scheme occurs (i.e., $h_s = h_w = h_e$ in Figure 2) which leads to a truncation error between that of nonequidistance and equidistance schemes, i.e., approximately proportional to h_θ^3. In order to realize this scheme, the radial mesh interval h_n (along a radius vector) is:

$$h_n = h_o/(1 - h_\theta)^n \qquad (7)$$

where n is the radial mesh point number. The first and also the smallest radial mesh interval is determined by

$$h_o = R_o/(\frac{1}{h_\theta} - 1) \qquad (8)$$

where R_o is the minimum radius which is most conveniently chosen as the apex radius for a spherical emitter while for a faceted emitter R_o can be chosen as the radius of the facet. From R_o and the maximum dimension of the gun R_m (i.e. the center of the spherical coordinate system to the most distant point), the required

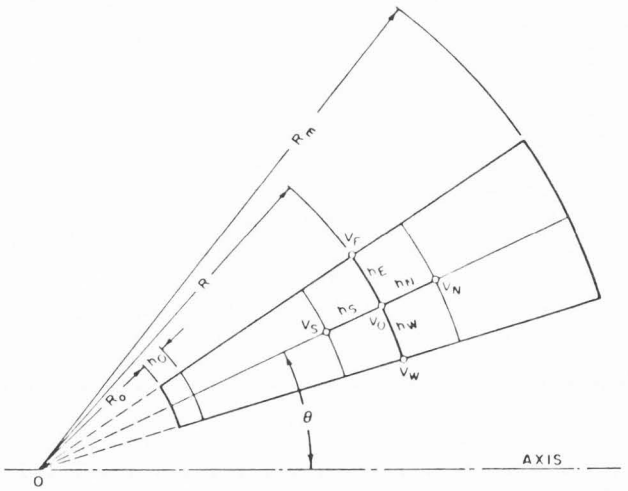

Figure 2.

Schematic representation of the mesh arrangement used in the SCWIM method. The minimum and maximum electrode dimensions are R_o and R_m respectively.

number of mesh points along a radius vector can be calculated by

$$N = \frac{\ln(R_o/R_m)}{\ln(1 - h_\theta)} - 1 \qquad (9)$$

Figure 3 shows the dependence of N on R_m/R_o for various values of h_θ. One notices that N increases very slowly with increasing R_m/R_o. For example, when R_m/R_o increases by four orders of magnitude (from 10^2 to 10^6), N increases only by a factor of 3 for $h_\theta = 0.1$. Generally, the number of radial mesh points approximately doubles when the ratio of geometrical sizes increases by two orders of magnitude. Because of this unique feature of SCWIM one is able to treat the entire gun at once without unreasonable demand

TABLE 2

Calculated emitter characteristics for the faceted ZrO/W(100) TFE source where ϕ = 2.8 eV, T = 1800 K. The minimum value of d_v and corresponding aperture half angle α_m are indicated for each value of r.

r(μm)	d_v (nm)	α_m (mr)	I' (mA/sr)	B (10^9 A/cm^2 sr)	J_c (A/cm^2)	F(V/A)
0.3	7.0	5.5	0.72	1.9	2.8×10^4	0.11
0.5	8.8	3.5	0.98	1.6	1.5×10^4	0.97
1.0	12.0	2.5	0.97	0.86	4.0×10^3	0.070
2.0	16.5	2.0	1.06	0.46	1.2×10^3	0.049
3.0	19.5	1.0	1.46	0.49	7.7×10^2	0.041

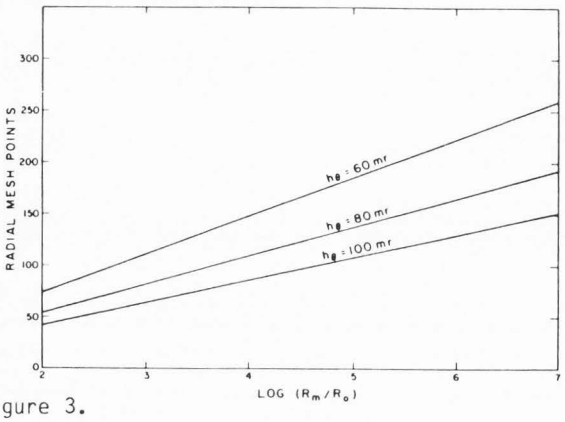

Figure 3. Plots of the number of radial mesh points N vs the electrode geometric ratio R_m/R_o for the SCWIM method. The angular mesh sizes h_θ are indicated.

on computer storage capacity. At the same time, the inaccuracy and complexity connected with the "successive magnification" approach are eliminated. In areas remote from the emitter the mesh size appears too large. However, the fields in such remote areas are fairly weak, therefore, the mesh arrangement in SCWIM matches the features of field emission guns very well.

By the use of Eq.(7), the axisymmetric Poisson equation in spherical coordinates, which is given by

$$\frac{\partial^2 V}{\partial r^2} + \frac{2}{r}\frac{\partial V}{\partial r} + \frac{1}{r^2 \tan\theta}\frac{\partial V}{\partial \theta} + \frac{1}{r^2}\frac{\partial^2 V}{\partial \theta^2} = -\frac{\rho}{\varepsilon_o} \quad , \qquad (10)$$

can be cast into a five-point difference form, which up to the fourth order term of a Taylor series, is given as follows (for notations see Figure 2):

$$V_o = B_1 \left(1 + \frac{h_\theta}{2\tan\theta}\right) V_E + B_1\left(1 - \frac{h_\theta}{2\tan\theta}\right) V_W + B_2 V_N + B_3 V + B_4 \frac{h_s^2 \rho}{\varepsilon_o} \qquad \text{(off-axis)}$$

$$V_o = B_{10} V_E + B_{20} V_N + B_{30} V_S + B_{40} \frac{h_s^2 \rho}{\varepsilon_o} \qquad (11)$$

(on-axis)

where ρ is the space charge density (negative value for electrons, positive for ions) in coulomb/m^3, $\varepsilon_o = 8.854 \times 10^{-12}$ F/m is the permittivity of free space, B_1, B_2, B_3, B_4 and B_{10}, B_{20}, B_{30}, B_{40} are functions of h_θ only.

That is to say, after h_θ is chosen, the B coefficients are constants, a factor which saves considerable computing time in electric potential iterations.

Virtual Source Size

Two experimental methods can be used to obtain values of d_v. Obviously, from Eq.(5) experimental measurements of d vs α can be used to evaluate d_v provided C_s and C_c are known or α is sufficiently small that the chromatic and spherical aberrations can be neglected. This is generally difficult since small values of d must be measured accurately. Another experimental method of measuring d_v is from the contrast patterns of a two beam interference behind an electrostatic biprism of the Mollenstedt type. This method was used to obtain a value of d_v = 31 nm for a room temperature W(310) FE source where α = 0.1 mr and I' = 7 mA/sr [11].

In addition to the experimental methods of obtaining d_v, computer trajectory calculations of the type first carried out by Weisner and Everhart can be employed [16]. Whereas the latter authors utilized an emitter shape that lends itself to an analytical solution for the electric potential, the SCWIM method can be applied to an emitter and extractor electrode of arbitrary shape.

The structure of field emission guns may vary a great deal. Among them a triode-type gun is most common. Figure 4 shows an example of a gun structure used with the ZrO/W(100) TFE source and, after some minor size modifications, with the LMIS. The suppressor electrode V_S can be used as a current control electrode and, in the case of the low work function ZrO/W(100) TFE, as a means of reducing thermal emission from the emitter shank.

ZrO/W(100) TFE Source

Following the approach of reference 16 we have used the SCWIM computer method to calculate

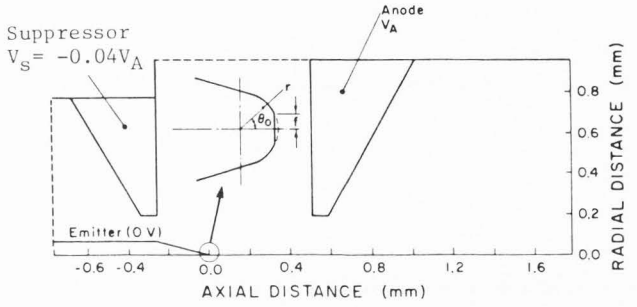

Figure 4.

Diagram of electrode configuration used in the gun structure for the ZrO/W TFE source. Insert shows an expanded view of the emitter of apex radius r for the rounded and faceted case. The launch angle for trajectories is θ and the flat radius is f.

d_V for the ZrO/W(100) TFE emitter for the realistic electrode configuration of Figure 4. As indicated in the inset of Figure 4 the ZrO/W(100) forms a large facet on the low work function (100) plane where the ratio of flat radius f to apex emitter radius r (when a rounded end form is assumed) is found experimentally to be f/r = 0.3. The reference plane from which extrapolation of trajectory tangents is made (see Figure 1) is R = 2.5 mm.

Values of d_V were calculated as a function of aperture angle α and emitter radius r for the faceted ZrO/W(100) TFE. The value of V_A was adjusted so that a constant value of $I' \cong 1$ mA/sr was maintained. An energy spread $\Delta V = 0.8$ eV, T = 1800 K and work function $\phi = 2.8$ eV were assumed for these calculations. The results given in Figure 5 and Table 2 show that d_V exhibits a minimum at small values of α. This is due to a balance between the diffraction aberration disk which varies as 1/α and the Gaussian, spherical and chromatic aberration terms all of which increase as various powers of α. Interestingly, the minimum value of d_V decreases with decreasing emitter size r; this is primarily due to a decrease in the Gaussian contribution since the spherical and chromatic terms are negligible. For emitter sizes typically used, e.g. r = 500 to 1000 nm, the minimum values of d_V are 9 to 12 nm. This corresponds to a cathode axial current density of $J_C = 4 \times 10^3$ to 1.5×10^4 A/cm^2 and an axial brightness $B = 0.9 \times 10^9$ to 1.6×10^9 A/cm^2 sr.

The unusually low values of J_C associated with I' = 1 mA/sr and the large values of B are due to the fact that the angular magnification $m \cong 0.22$ is unusually low. This follows from Eq.(2) where J_C is shown to vary inversely with m. For rounded emitter shapes typically $m \cong 0.5$ so that values of J_C are correspondingly small for a specific value of I'.

Using the same emitter parameters, except for a rounded end form as shown in Figure 4, the Figure 6 results were obtained. Again, the calculated values d_V show a minimum as α is varied. Plotting the minimum values of d_V vs r, we obtain the results shown in Figure 7 for both the faceted and rounded end form. From the latter

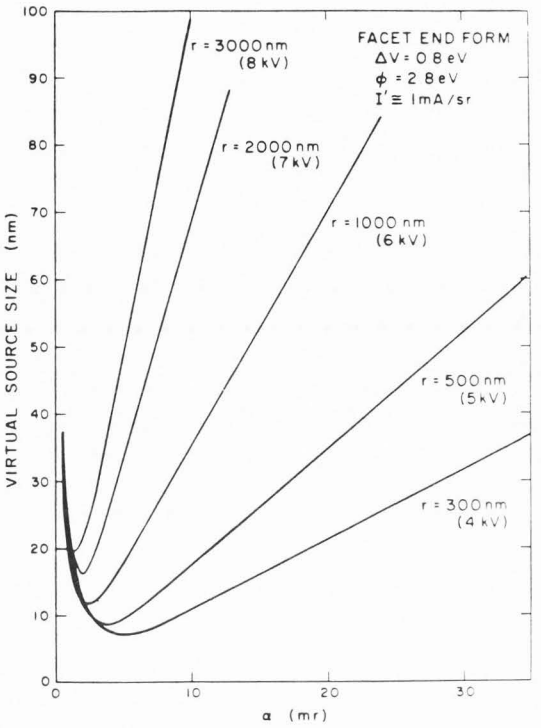

Figure 5.

Plot of virtual source size vs beam angle for the facet end form emitter for the indicated emitter radii and anode voltages.

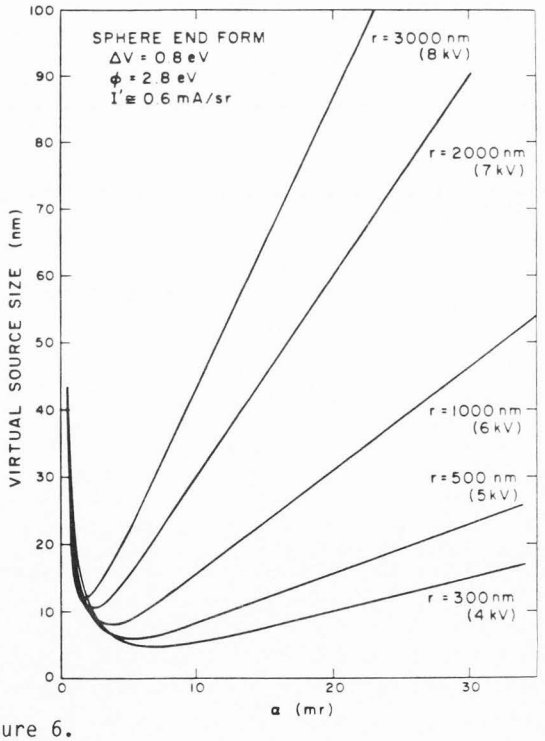

Figure 6.

Plot of virtual source size vs beam angle for the round end form emitter for the indicated emitter radii and anode voltages.

TABLE 3

Effect of Facet Formation on Angular Intensity for the ZrO/W(100) Emitter Where ϕ = 2.8 eV

Emitter Radius (μm)	Anode Voltage (kV)	Apex Field (V/Å)	J (A/cm^2)	m	I'(mA/sr)
0.3 (round)	4	0.14	1.40×10^5	0.45	0.61
0.3 (facet)	4	0.11	3.58×10^4	0.20	0.72
1.0 (round)	6	0.089	1.36×10^4	0.50	0.54
1.0 (facet)	6	0.070	5.29×10^3	0.22	0.97
3.0 (round)	8	0.053	2.05×10^3	0.55	0.62
3.0 (facet)	8	0.041	1.04×10^3	0.24	1.46

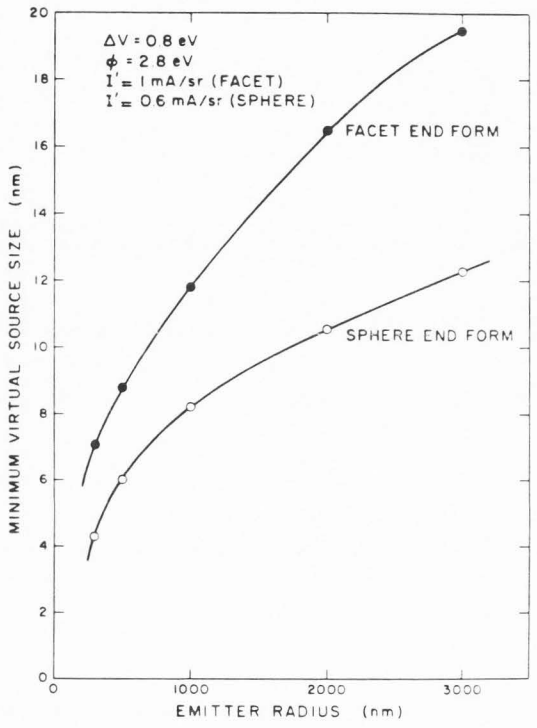

Figure 7.

Plot of the minimum virtual source size vs emitter radius for the facet and round end forms.

results we may conclude that the effect of the facet is to increase d_V by ~ 75% throughout the range of r values investigated.

At present no direct experimental measurement of d_V for the ZrO/W(100) TFE has been carried out. Indirect measurements involving the use of Eq.(5) to compare predicted and experimental values of d in focused beam studies using the ZrO/W(100) TFE source generally support a value of $d_V \leq 20$ nm for r = 1 μm, I' = 1 mA/sr and α = 2 to 6 mr [14,15].

LMIS

The value of d_V for the LMIS can be determined by the SCWIM computer program in the same manner as described in the previous section for the ZrO/W(100) TFE source. The primary modification of the input parameters is to the values of F and r which become F $\cong$ 2 V/Å and r $\cong$ 10 nm. Unfortunately, the detailed shape of the emitting portion of the LMIS is not well known so a model calculation using the SCWIM computer program would be premature. Originally the shape was believed to be a 45° half angle cone truncated by a hemispherical emitter of radius < 10 nm. More recent computer modeling of the emission characteristics and stability criteria of the liquid cone has suggested that the apex of the 45° half angle cone has an elongation of the order of 0 to 100 nm depending on the current [5,6]. This has been confirmed recently by TEM of an operating LMIS [2].

Using an elongated cone shaped emitter and the SCWIM program a preliminary estimate of d_V = 0.2 nm was obtained for a Ga^+ source [5]. The very small value of d_V for the LMIS is due to the elimination of diffraction aberration and the small transverse velocity associated with field evaporated ions. Nevertheless experimental measurements of d_V using results of focused ion beam measurements at small values of α suggest the $d_V \cong$ 50 nm [9,12]. This large discrepancy between prediction and experiment is not completely clear at this time, however if further results confirm this discrepancy its origin may be due to the strong Coulomb interaction known to occur in the high charge density region within a few emitter radii from the emitter surface. This Coulomb interaction comes about due to the random fluctuations in the charge density and manifests its effect in terms of an increase in the energy spread and d_V. A considerable discussion of this effect has taken place in connection with electrons and is known as the "Boersch effect." More recently this important effect has been considered in connection with high J point sources of electrons and ions [7,17] and at present is not included in the SCWIM program.

Angular Intensity

According to Eq.(2) the angular intensity I' of a point emitter is determined by the emitter current density, which is intrinsic to the emission process, and the angular magnification m, which is determined by the emitter and surrounding extractor electrode shape and potentials. The value of m can be determined by SCWIM via Eq.(1); the dependence of J on F, T and ϕ requires a theoretical model of the emission mechanism.

For electron emission the $J(\phi,F,T)$ relationship can be determined either numerically or from analytical expressions which cover the

range of F, ϕ and T extending from pure field emission at high F and low T to pure Schottky emission at low F and high T. The general emission equation based on the Sommerfeld model of metals is given by

$$J(T,\phi,F) = \int_0^\infty J(\varepsilon)d\varepsilon \qquad (12)$$

where ε is the electron energy relative to the Fermi level E_F and

$$J(\varepsilon) = \frac{4\pi me}{h^3} f(\varepsilon) \int_0^{E_F + \varepsilon} D(W)dW \qquad (13)$$

where $f(\varepsilon)$ if the Fermi-Dirac function, W is the kinetic energy associated with the normal component of electron momentum and D(W) is the one-dimensional transmission function [10]. The numerical integration of Eq.(12) is performed in the SCWIM program for electrons thereby providing a value of J as a function of the local field.

For the LMIS an analytical relationship for J is not presently available and is not likely to be developed due to the uncertainty of the emitter shape. Nevertheless, using a dynamic model for stabilization of an elongated cone, a field evaporation model for ion formation and the SCWIM program to calculate trajectories an empirical relationship between I' and J has been developed [6].

ZrO/W(100) TFE Source

Trajectories were calculated for the faceted and rounded end form using the SCWIM program and the Figure 4 electrode structure. The results listed in Table 3 show that the value of m for the faceted end form is a factor of 2 lower than the rounded end form.

Thus, the value of J_C for a specified I' is reduced by a factor of 4 due to the facet and the current density to achieve ~ 1 mA/sr emission intensity remains low (< 10^4 A/cm^2) throughout the range of practical emitter radii. Empirically it has been found that Eq.(2) is of the form

$$I' = 20.42\ J_C\ r^{1.87}$$

for the faceted end form emitter. The low values of J_C required to obtain a value of I' $\cong$ 1 mA/sr for r > 0.3 μm mean that the continuum space charge effect on trajectories and surface field is negligible as shown earlier [4].

Typically, the ZrO/W(100) cathode can be operated stably for values of I' and r in the range of 0.1 to 2 mA/sr and 0.3 to 1.5 μm respectively. The apparent source brightness, given by

$$B_A = \frac{4I'}{\pi d_V^2},$$

can be calculated for I' = 1 mA/sr and $d_V \tilde{=}$ 10 nm to be $B_A = 1.3 \times 10^9$ A/cm^2 sr.

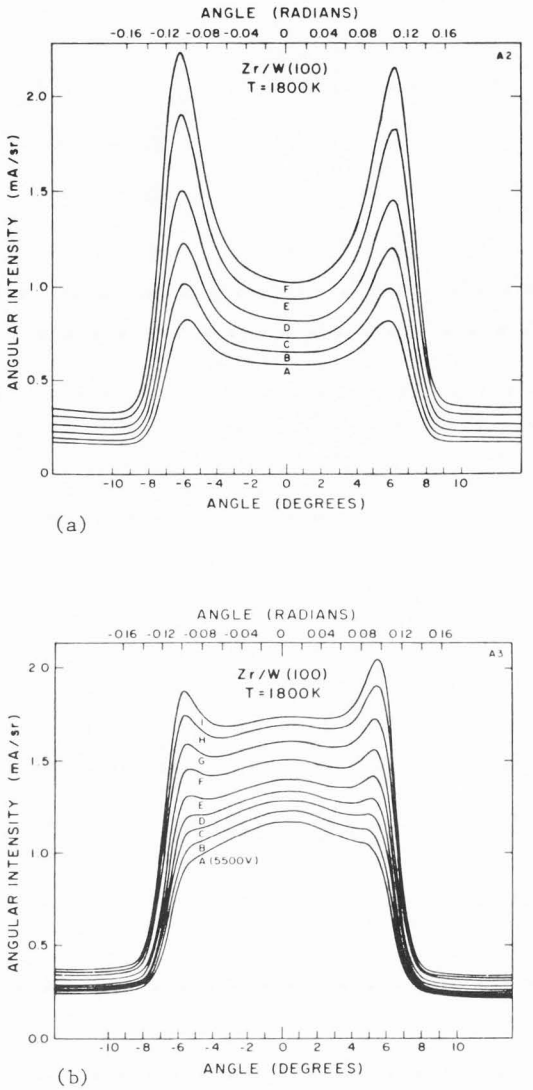

Figure 8.

Experimental values of the angular current distribution for a ZrO/W(100) TFE source at 100 V anode voltage increments: (a) Emitter radius was 0.8 μm and anode voltage for curve A was 4300 V; (b) Emitter radius was 2.0 μm and anode voltage for curve A was 5500 V.

The experimental angular intensity distribution for two emitter radii is given in Figure 8. In Figure 9 are the predicted angular intensity distribution curves using the SCWIM program for a 0.3 and 3.0 μm faceted emitter when the axial value of I' $\cong$ 1 mA/sr. The predicted and experimental curves show remarkably good agreement. The high value of I' at the edge of the facet is due to the locally high field strengths. However, as r increases or V decreases the emission mode shifts from TF to pure Schottky emission thus reducing the effect of local field on the emission distribution.

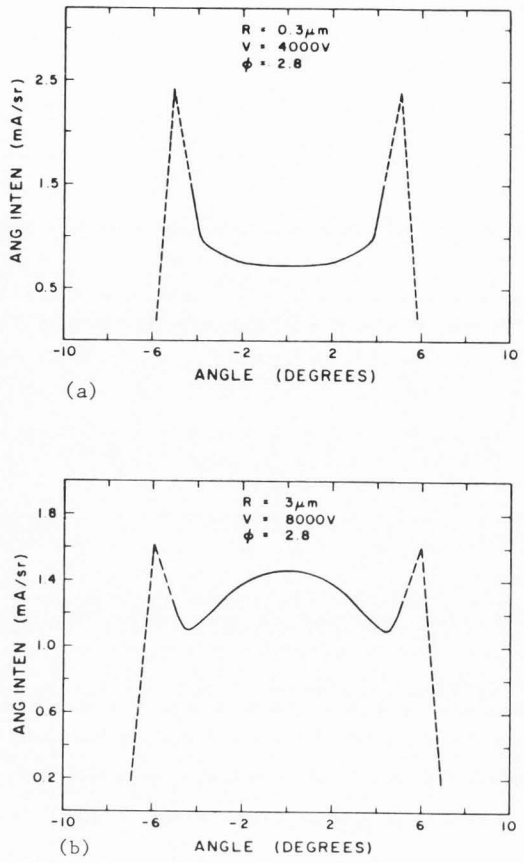

Figure 9.
Calculated angular distribution curves for a faceted emitter using the SCWIM computer program: (a) Emitter radius was 0.3 μm; (b) Emitter radius was 3.0 μm.

LMIS

The angular intensity distribution for the LMIS is similar for all sources and typically shows a uniform distribution whose angular divergence increases with current and mass. Figure 10 shows the current dependence of the angular distribution for a Ga LMIS. The dashed line is a theoretical prediction based on an elongated emitter shape using the SCWIM program for trajectory calculation [6]. Figure 11 shows the mass dependence of the full width at half maximum of the angular divergence. For a low mass LMIS such as Al the value of I' at the onset of current is ~ 40 μA/sr. In contrast for a Bi LMIS the onset value is I' ≅ 10 μA/sr. Because of the small size of the emitting area of the LMIS, the current density is remarkably large--believed to be in excess of 5×10^8 A/cm^2. Thus, space charge effects in the beam are important. Nevertheless the analysis shows that the increase in beam divergence with current and mass is due to both space charge effects and trajectory modification due to elongation of the cone shaped liquid metal emitter [6].

The substantial decrease in experimental axial values of I' with mass for I = 10 μA is shown in Figure 12. This result is in agreement with the Figure 11 results and is due to the mass

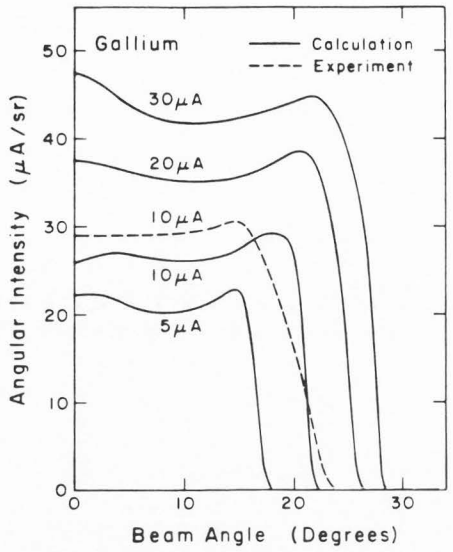

Figure 10. Calculated angular intensity in the exit plane as a function of beam angle for a Ga source at currents between 5 and 30 μA. The experimental results for a Ga LMIS at 10 μA are also shown.

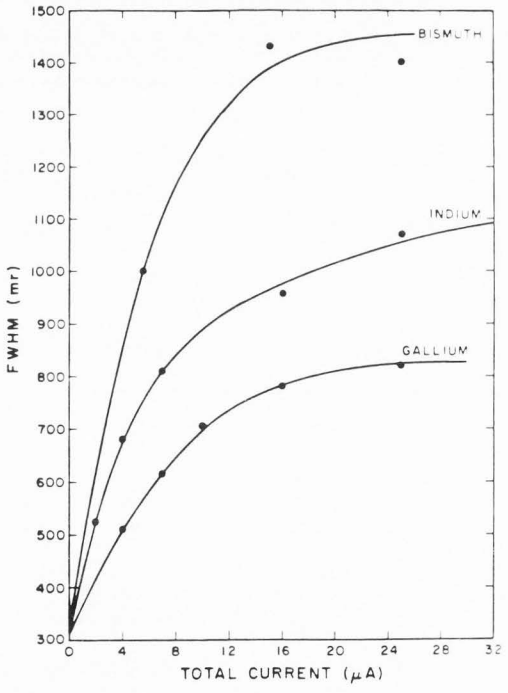

Figure 11. Curves show the experimental values of full width at half maximum (FWHM) of the Figure 10 angular distribution curves vs current for the various LMIS.

dependent space charge effects and trajectory modification as mentioned earlier. Using the elongated, cone shaped model of the LMIS and the SCWIM program, the calculated curve in Figure 12 for I' vs mass at I = 10 μA shows good agreement

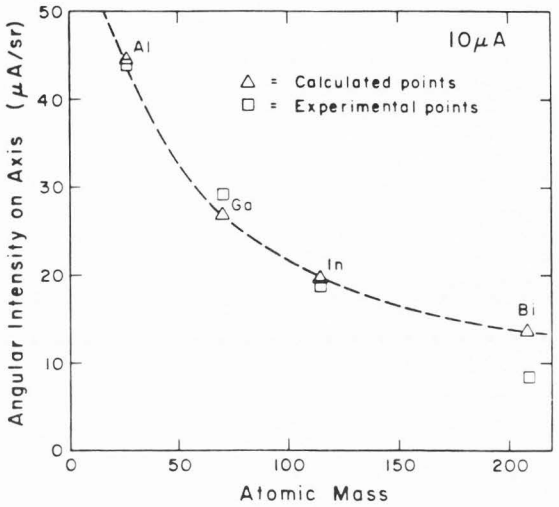

Figure 12. Points show the experimental and calculated (using the SCWIM program) values of the axial angular intensity vs atomic mass for a beam current of 10 μA.

with experimental results [6].

If one assumes the previously mentioned experimental values of d_v = 50 nm and I' = 20 μA/sr, then one obtains a source brightness for a Ga LMIS of B = 1 × 10^6 A/cm^2 sr. Although higher values of B can be obtained at larger values of I', as will be shown below, the increase in beam energy spread negates any optical advantage of larger B.

Energy Distribution

According to Eq.(6) the beam current in a focused beam dominated by chromatic aberration is inversely proportional to ΔE^2. In addition to an intrinsic energy spread ΔE_i, it has been found that an additional, current and emitter radius dependent contribution $\Delta E_C(I,r)$ occurs for all high field sources. The origin of ΔE_C for high field, point sources has been a matter of some discussion and is believed to be due to relaxation of initial Coulomb potential energy caused by random density fluctuations of the charged particles [7,17].

ZrO/W(100) TFE Sources

From the numerical integration of Eq.(13) the theoretical energy distribution and, hence, $\Delta E_i(\phi,F,T)$ can be obtained for a FE source. The results of such a calculation are given in Figure 13 as a function of J (obtained from Eq.(12)) for specified ϕ and J values. For emitters with ϕ < 3.0 eV and J < 10^5 A/cm^2 and operating temperature T $\gtrsim$ 1500 K the value of ΔE_i decreases with increasing T. Thus for typical operating parameters of the ZrO/W TFE ($\phi \cong$ 2.8 eV, J = 10^3 to 10^5 A/cm^2, T = 1800 K) the value of ΔE_i < 0.6 eV. On the low temperature side of the maxima in the Figure 13 curves the emission mode is primarily field emission, whereas on the high temperature side of the maxima the emission mode is primarily Schottky emission and ΔE_i becomes small and approaches kT. The unique

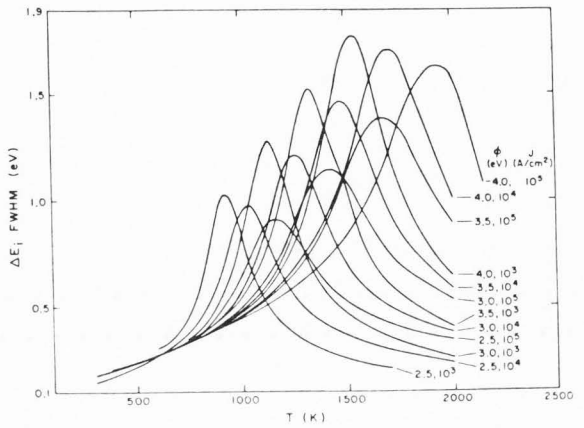

Figure 13. Calculated values of the full width at half maximum of the total energy distribution curves as a function of temperature. The plots are given for the indicated values of work function ϕ and current densities J.

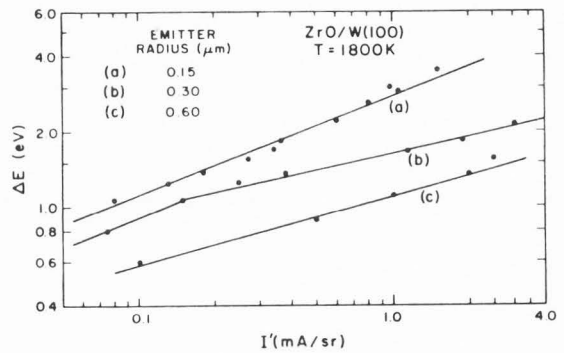

Figure 14. Experimental values of the full width at half maximum of the energy spread ΔE vs angular intensity I'. The results are given for three values of emitter radius.

operating parameters of the ZrO/W(100) emitter allow it to function as a pure FE at low T and high F or as a pure Schottky emitter at high T and low F.

Figure 14 shows experimental values of ΔE vs I' for ZrO/W(100) emitters of differing emitter radius. For values of I' $\lesssim$ 0.1 mA/sr ΔE approaches the theoretical value of $\Delta E_i \lesssim$ 0.6 eV; however as I' increases or as r decreases ΔE increases due to the aforementioned stochastic Coulomb interactions. Thus, in order to reduce the chromatic aberration contribution at high values of I' the ZrO/W(100) emitter radius should be large. In practice typical values of r are in the range 0.5 to 1.0 μm and at I' = 1 mA/sr the relatively low values of J = 1.5 × 10^3 to 5.4 × 10^3 A/cm^2 are obtained.

LMIS

As in the case for electron emission from the ZrO/W(100) TFE it has been observed that the LMIS also shows an increase in the FWHM of the total energy distribution (TED) with current. Figure 15

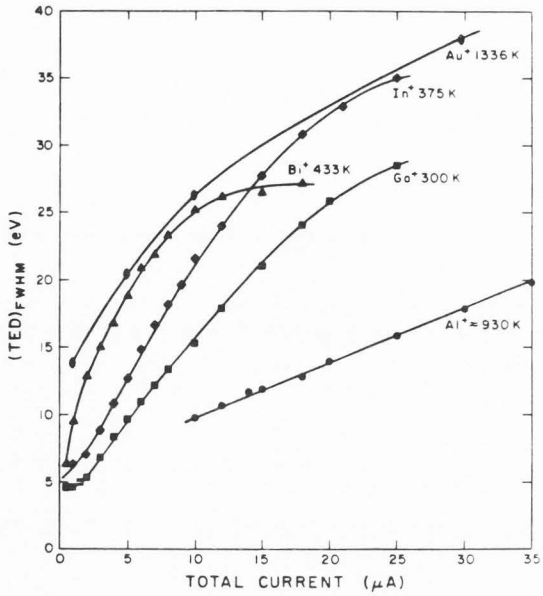

Figure 15. Experimental values of the full width at half maximum of the total energy distribution vs current for the indicated ions of a single component LMIS.

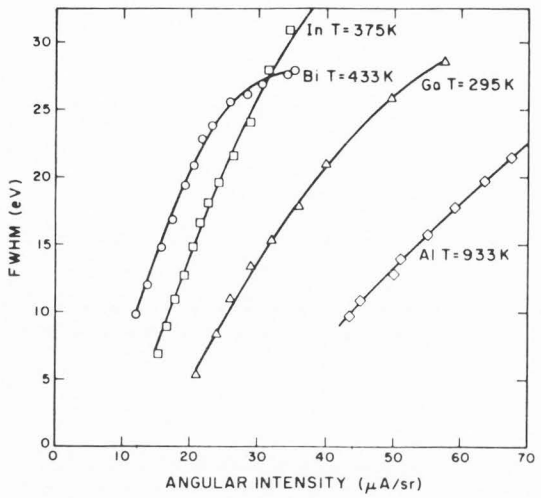

Figure 16. Experimental values of the full width at half maximum of the total energy distribution vs angular intensity for the singly charged ions of the indicated single component LMIS.

shows the experimentally observed variation of ΔE with total source current for several pure metal LMIS [12]. As $I \rightarrow 0$ the value of $\Delta E \rightarrow 5$ eV for nearly all the LMIS investigated whereas at high values of I a strong mass dependence of the ΔE values is observed.

The mass dependence of the ΔE values can be seen more dramatically in Figure 16 where its variation with the axial value of I' is shown. According to Eq.(6) the source figure of merit for chromatically limited micro-focus applications is given by the value of $I'/\Delta E^2$ when $d/m > d_v$. Clearly, from Figure 16 one can see that $I'/\Delta E^2$ decreases rapidly with increasing mass at a fixed value of ΔE. For example, at $\Delta E = 10$ eV the figure of merit values for Al and Bi LMIS are 0.45 and 0.1 $\mu A/sr\ (eV)^2$ respectively.

Although few theoretical analyses of the energy broadening of LMIS with increasing I and mass have been carried out to date, it is generally believed that, as in the case of the TFE source, a stochastic Coulomb interaction in the beam is the primary mechanism responsible for the Figures 15 and 16 results.

Conclusions

The analysis of two promising electron and ion field sources shows that high angular intensities and small values of virtual source size can be expected. Typically source brightness values in excess of 1×10^6 and 1×10^9 A/cm^2 sr can be obtained from the LMIS and ZrO/W TFE electron source. Because of the increase in energy spread with angular intensity for these sources, one must carefully optimize the source operating conditions for a specific optical column. In addition, for LMIS an increase in ion mass reduces angular intensity and increases energy spread for a given source current.

Acknowledgments

This work was supported in part by NSF grant ECS-8206796. The author is grateful to A. Bell for helpful discussions and to G. Schwind for obtaining many of the experimental results.

References

[1] Bell A, Schwind G, and Swanson L. (1982). The Emission Characteristics of an Al Liquid Metal Ion Source. J. Appl. Phys. 53, 4602-4605.

[2] Gaubi H, Sudraud P, Tence M, and van de Walle J. (1982). Some New Results About In Situ TEM Observations of the Emission Region in LMIS, in: Proc. 29th Int. Field Emission Symposium, Goteborg, Sweden, H. O. Andren and N. Norden (ed), Almqvist and Wiksell Int., Stockholm, 357.

[3] Kang N, Orloff J, Swanson L, and Tuggle D. (1981). An Improved Method for Numerical Analysis of Point Electron and Ion Source Optics. J. Vac Sci. Technol. 19, 1077-1081.

[4] Kang N, Tuggle D, and Swanson L. (1983). A Numerical Analysis of the Electric Field and Trajectories With and Without the Effect of Space Charge for a Field Electron Source. Optik 63, 313-331.

[5] Kang N, Swanson L. (1983). Computer Simulation of Liquid Metal Ion Source Optics. Appl. Phys. A30, 95-104.

[6] Kingham D, Swanson L. (in press). Shape of a Liquid Metal Ion Source; A Dynamic Model Including Fluid Flow and Space-Charge Effects. Appl. Physics A.

[7] Knauer W. (1981). Energy Broadening in Field Emitted Electron and Ion Beams. Optik 59, 335-354.

[8] Komuro M. (1983). Liquid Metal Ion Sources--Mass Spectrometry Study of Ga, In, Sn, Au, Pb, and Bi. Proc. Int. Ion Eng. Congress, Kyoto, 337-348.

[9] Komuro M, Hiroshima H, Tanoue H, and Kanayama T. (1983). Maskless Etching of a Nanometer Structure by Focused Ion Beams. J. Vac. Sci. Technol. B1, 985-989.

[10] Murphy E, Good R. (1956). Thermionic Emission, Field Emission, and the Transition Region. Phys. Rev. 102, 1464-1473.

[11] Speidel R, Kurz D. (1977). Richtstrahlwertmessungen an einem Strahlerzeugungssystem mit Feldemissionskathode. (Brightness measurements at an electron gun with field emission cathode.) Optik 49, 173-185.

[12] Swanson L. (1983). Liquid Metal Ion Sources: Mechanisms and Applications. Nucl. Inst. Meth. Phys. Res. 218, 347-353.

[13] Swanson L, Bell A. (1973). Recent Advances in Field Electron Microscopy of Metals. Adv. Electronics & Electron Phys. 32, 193-309.

[14] Swanson L, Tuggle D, and Li J. (1983). The Role of Field Emission in Submicron Electron Beam Testing. Thin Solid Films 106, 241-255.

[15] Tuggle D, Swanson L, and Orloff J. (1979). Application of a Thermal Field Emission Source for High Resolution, High Current e-Beam Microprobes. J. Vac. Sci. Technol. 16, 1699-1703.

[16] Wiesner J, Everhart T. (1973). Point-Cathode Electron Sources--Electron Optics of the Initial Diode Region. J. Appl. Phys. 44, 2140-2148.

[17] Yau Y, Groves T, and Pease R. (1983). Space Charge Effects in Focused Ion Beams," J. Vac. Sci. Technol. B1, 1141-1144.

Discussion with Reviewers

P. B. Sewell: For the computations of Fig. 13, work function values of 3.5 and 4.0 are used, rather than values close to 2.8 eV as generally used for the ZrO/W(100) emitter. Is there any reason for this? Also, with reference to the results of Fig. 13, could you comment further on the physical origin of the increase in ΔE_i between the extreme values for the field emission and Schottky modes?

Author: The values of work function used in Fig. 13 vary from 2.5 to 4.0 eV. The value typically measured for the ZrO/W(100) emitter at room temperature is 2.7 ± .2 eV. The maximum in the Fig. 13 curves is due to broadening with increasing temperature of the occupied electron states above the Fermi level from which electrons tunnel. At low temperatures and high electric field ΔE_i is small due to the fact that few states above the Fermi are occupied and at high temperatures ΔE_i is small because the field is low and all electrons are forced surmount the work function barrier.

E. Munro: Table I - it was not very clear to me what the angle α represents in this table. Is it the angle at which electrons are emitted from the cathode, or the angle at which they emerge from the gun? Also the meaning of V was not clear to me, I presume it means the beam voltage at emergence from the gun?

Author: The angle α is the beam angle, i.e. the angle when the electrons emerge from the gun. The symbol V refers to the beam voltage as the particles emerge from the gun region.